Comparison of the cervical spine bony kinematics for female PMHS with the virtual EvaRID dummy under whiplash loading.

Andreas J. Gutsche, Ernst Tomasch, Mario Darok, Wolfgang Sinz, Iztok Ciglaric, Dean Ravnik, Hermann Steffan

Abstract The recently developed EvaRID dummy model allows virtual investigations of female vehicle occupants. Females in general show an increased risk of sustaining whiplash-associated disorders in rear impacts. To verify the performance of the EvaRID model during its development a comparison with volunteer tests was performed. The load (e.g. delta-v) on volunteers is limited due to injury risks. Also, the kinematics of vertebral bodies was not recorded in these studies. Thus, two female post mortem human subjects (PMHS) matching the anthropometry of 50th percentile females were tested, in two different setups with and without head restraint and two different acceleration pulses (Euro NCAP mid and high severity). The PMHS were equipped with several accelerometers. Lateral overview high-speed videos and detailed high-speed radiographic videos of the vertebral bodies were captured. From the radiographic videos, trajectories of the vertebrae were extracted and kinematics compared with Finite Element Analysis. A good correlation of the global kinematics for the head and upper body and also for the behaviour of the single vertebrae of EvaRID compared to the PMHS' vertebras was found. Furthermore the study shows that EvaRID seems as representative in behaviour compared to female PMHS as the BioRID model is for male PMHS.

Keywords Female whiplash, high speed x-ray, neck injury, PMHS, **r**ear impact

I. INTRODUCTION

Numerous studies have pointed out that female vehicle occupants show an up to three times higher risk of sustaining whiplash-associated disorders (WAD) than males [1-13]. The real cause for this is currently still not completely understood. Nevertheless, most research done in this field targets 50th percentile male occupants. Furthermore, as [14] shows, recent protective systems seem to increase protection for male but not for female occupants to the same extent. Among efforts to amend this situation, within the recently completed ADSEAT project [15], a female finite element dummy model for whiplash assessment, the so-called EvaRID (Eva - indicating female, RID - Rear Impact Dummy), was developed. Female validation data however were not available. Also a physical device of the EvaRID dummy is not yet available for comparison. Moderate volunteer sled tests (delta-v < 7km/h) with females were conducted during the model development to verify the functionality and biofidelity of the designed model. Higher delta-v loadings were not applied to volunteers. Due to the lack of a physical EvaRID dummy and severity limitations of loading on female volunteers, no appropriate set of data at relevant loading levels (e.g. Euro NCAP medium or high severity pulse) was available. Thus, a comparison with Post Mortem Human Subjects (PMHS) seemed reasonable and necessary. Already [16] showed with PMHS tests and x-ray videos that different loads are applied during rear-end impacts. These loads were identified and divided in three stages (a flexural deformation until approximately 100 ms, an extensional motion of the lower cervical spine until about 130 ms and an extensional deformation of the entire cervical spine until 180 ms). The method with x-ray videos and metallic markers proved to be of great value for kinematic analysis of bony structures. In this investigation, however, no focus on gender differentiation was set. In addition, the level of loading, which is described as below delta-v of 7km/h in the study of [16], is not in the range of current consumer tests.

The aim of this study was to show whether the virtual female rear impact dummy model EvaRID is a suitable

A. J. Gutsche is Doctoral student in Engineering Sciences at Graz University of Technology in Austria (phone: +43 316 873 30319, fax: +43 316 873 1030319, andreas.gutsche@tugraz.at). E. Tomasch, W. Sinz, I. Ciglaric, H. Stefan - Graz University of Technology in Austria. M. Darok – Medical University of Graz in Austria. D. Ravnik - University of Ljubljana, Ljubljana, Slovenia.

tool to represent female occupants (in this case PMHS) during rear-impact collisions.

II. METHODS

Experimental Testing

For this study a series of sixteen sled acceleration tests was performed. Two male and two female PMHS matching a 50th percentile male and female, respectively [17], were tested (Appendix 1). The main focus of this study is on females and the majority of further analysis is limited to data from female cases (Table 1). The tests were performed on a computer-controlled acceleration sled device powered by high pressure air. The device, as shown in Figure 1, can reproduce the relevant acceleration pulses very accurately, such as used in the European New Car Assessment Protocol (Euro NCAP) [18]. The acceleration pulses were chosen to fit the Euro NCAP medium (International Insurance Whiplash Prevention Group, IIWPG 16 km/h) and high severity (Swedish Road Administration, SRA 24 km/h) pulse.

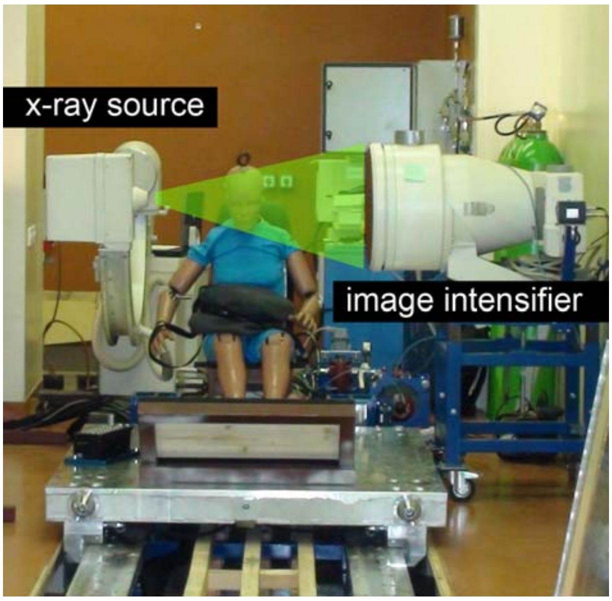

Figure 1. Acceleration sled device with x-ray source, image intensifier and high speed camera.

The sled device was equipped with a rigid ECE-R16 seat [19]. It was slightly modified so it could hold a head restraint in the corresponding tests. The head restraint used was a simple standard foam-only, height-adjustable device. The head restraint, when present, was positioned so that the top of the head restraint aligned with the top of the head of each PMHS. The distance between head and head restraint was set to 80 mm - 100 mm. A simple three-point safety belt system was added to secure the PMHS on the seat during the rebound phase.

Each PMHS was tested in four different configurations as listed in Table 1. After each test, forensic doctors examined the PMHS for trauma such as fractures or dislocations. For each pulse and PMHS one test with and one test without head restraint were performed. Tests without head restraints were conducted in order to gather longer kinematic trajectories. The PMHS were maintained in their seated posture prior to t-zero with supportive objects such as low density foams. Furthermore, the head and neck posture was secured with a belt system attached to an electromagnetic release, which was triggered 5 ms prior to t-zero. The subjects were equipped with three tri-axial accelerometer sensors (DSD200, DSD, Austria). One sensor was attached to the sternum in front of the torso in the mid-sagittal plane. Another sensor was attached to the T1 vertebral body on the back of the neck in the mid-sagittal plane and the third to the left side of the head (skull) at the approximate x and z position of the centre of gravity of the head. One uniaxial acceleration sensor (Vibration Sensor - Model 1201 Accelerometer, Measurement Specialties, USA) was attached to the ECE-R16 seat to monitor the acceleration pulse of the sled device. Data were recorded using a data acquisition unit (DAU - Mini DAU K3700, KT Automotive, Germany) at a rate of 20 kHz.

TABLE 1

Test Matrix PMHS Tests

PMHS	Config.	Gender	Acceleration	Head Restraint
1	1	Female	IIWPG 16 km/h	In place
	3		SRA 24 km/h	In place
	2		IIWPG 16 km/h	Removed
	4		SRA 24 km/h	Removed
4	1	Female	IIWPG 16 km/h	In place
	2		SRA 24 km/h	In place
	3		IIWPG 16 km/h	Removed
	4		SRA 24 km/h	Removed

In addition to acceleration lateral high-speed videos (1000 fps) of the torso, neck and head were recorded. For this purpose, two high-speed camera systems also triggered by the sled system were used (SpeedCam MacroVis, Weinberger, Germany). Detailed high-speed radiographic videos (500 fps) of the vertebral bodies were captured.

For radiography, a modified c-arch x-ray system (BV 25 Family-N/HR Philips, The Netherlands) was used. The picture intensifier had a diameter of approximately 400 mm (SIRECON, Siemens, Germany). The camera system of the c-arch x-ray system was replaced with a high-speed camera system (SpeedCam MiniVis, Weinberger, Germany). High-speed videos, high-speed radiographic videos and measurements were synchronised. To increase contrast, vertebral bodies were marked with small screws as shown in Figure 2. These screws were inserted directly into the bone.

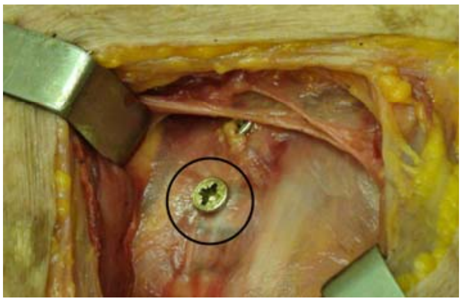

Figure 2. Screws marking single vertebral bodies for contrast on x-ray radiography

The screws were positioned directly into the bony material of the vertebral bodies on the front side of the neck in the mid-sagittal plane. The positions for the markers were chosen so that the screws describe the same motion as the vertebral bodies in which they were placed. The ligamentum longitudinale anterius was punctured in this process. Damage to the ligaments was prevented as far as possible. These markers for vertebral bodies could be used as targets for a slightly modified target tracking. All tests were conducted under approval of the responsible ethics committee of the republic of Slovenia (Reference Number 47 10.3.10).

Finite Element Methods

For Finite Element Methods (FEM) the proprietary FEM code LS-Dyna (Version 971 R5.1.1) was used. Within this investigation, the newly developed finite element dummy model EvaRID (ADSEAT-EvaRID Model LS-Dyna Release Version 1.0 August 2010 [17]), representing the 50th percentile female occupant (Figure 3), was used. Simulations were conducted applying two of three Euro NCAP pulses, the medium severity and high severity pulse, which were also used during PMHS testing. Data were logged and injury criteria were computed. Of special interest was the kinematic behaviour of the vertebral bodies of the virtual EvaRID model for the comparison with bony kinematics gathered from PMHS high-speed x-ray videos.

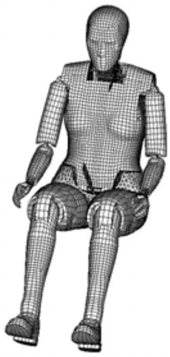

Figure 3. EvaRID FEM model [17]

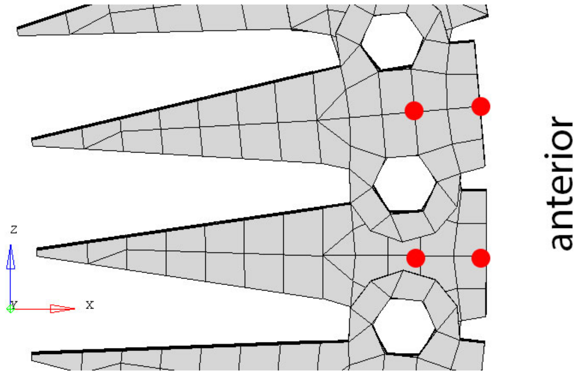

Figure 4. Example of nodes tracked for trajectory

In this case, two nodes aligned on the mid-sagittal plane on the mid-horizontal plane of each vertebral body were tracked and analysed, as exemplified in Figure 4. Complementary simulations with the BioRID II model (FAT LS-DYNA BioRID II Model - Version 2.5, LS-Dyna, DYNAmore GmbH, Sept. 2011) were conducted for a qualitative comparison with the female EvaRID model. For these finite element analyses (FEA), the IIWPG 16 km/h and SRA 24 km/h Euro NCAP pulses were also used.

Analysis and Comparison

From the high-speed x-ray videos, trajectories of vertebral bodies were generated using target tracking. These data from PMHS testing were compared with trajectories extracted from the FEAs. The comparison gives a general overview of the kinematic behaviour of PMHS and the FEA dummy, i.e. of their cervical vertebral bodies.

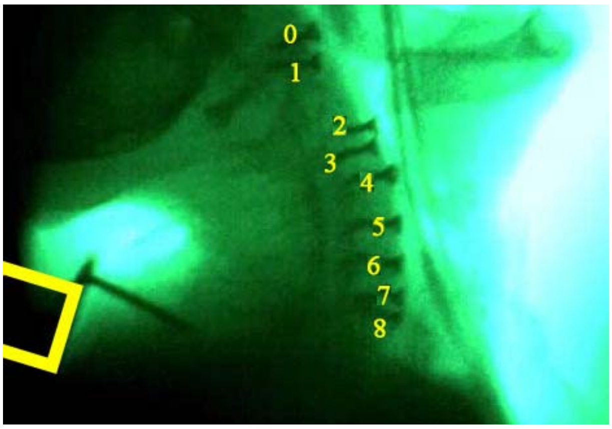

Figure 5. Example of radiographic picture of a high speed video with numbered markers for target tracking and T1 accelerometer

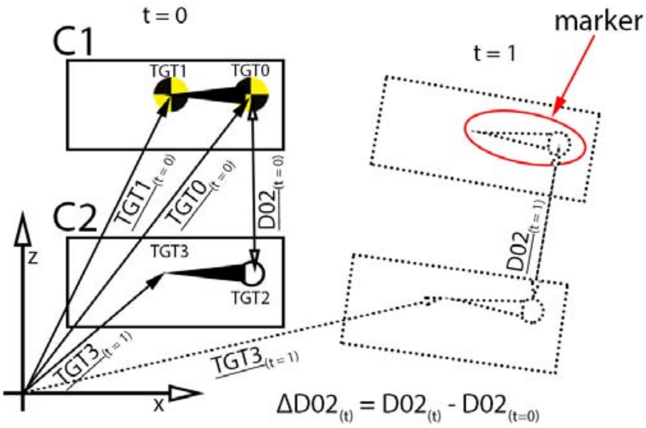

Figure 6 Determination of positions of traced targets and distances between them

In Figure 5 an example picture with the numbered markers for the trajectory tracking is given. In some x-ray videos, the tip and the head of the marker could be tracked; in some, only the head was clearly visible for tracking. Also the T1 accelerometer can be found in the lower left corner of the picture (indicated with a yellow frame). Radiographic pictures for all PMHS tests can be found in Appendix 32 through Appendix 39. The picture area of all high-speed x-ray videos is limited by the diameter of the image intensifier. In this picture all mounted markers (screws) are visible. Depending on the test configuration and PMHS, up to twelve targets (TGT) were used, since head and tip of each marker was tracked where possible as indicated in Figure 6. Not all markers are visible in all tests for a sufficient period of time, thus not all trajectories are available in some configurations. For each captured picture the positions of each available target in the picture were measured as shown in Figure 6. A coordinate system which is fixed to the picture area (origin at pixel x= 0 and y= 0) was used as a global system. Markers as described were placed in each vertebral body. Each marker was assigned with two targets, one the leading head and one the following tip of the pin used as traceable targets. Where possible, all targets were tracked by vectors as shown in Figure 6, e.g. TGT3$_{(t=0)}$. Due to restrictions in picture quality not all of the tips of the markers for all PMHS could be tracked. The dimensions of the markers were known, thus the coordinates could be determined and transformed to mm. One pixel of the high-speed x-ray video represented approximately 0.37 mm.

III. RESULTS

The tracking of the vertebral bodies during the rear impact was analysed for comparison. In the following Figure 7 and Figure 8 examples are given for one PMHS test and one FEA simulation, respectively. The graphs show the trajectory of the targets (vertebral bodies) during the whiplash motion in a coordinate system fixed to the picture intensifier. The extent of available data for all PMHS tests is limited by the size of the picture intensifier. The values on the abscissae represent the forward movement of the targets in x-direction, values on the ordinate the corresponding z-oriented upward movement. The lines in these graphs represent the curves of the tips of the vectors described as TGT0$_{(t)}$ through TGT11$_{(t)}$ as displayed in Figure 6 during the whiplash loading.

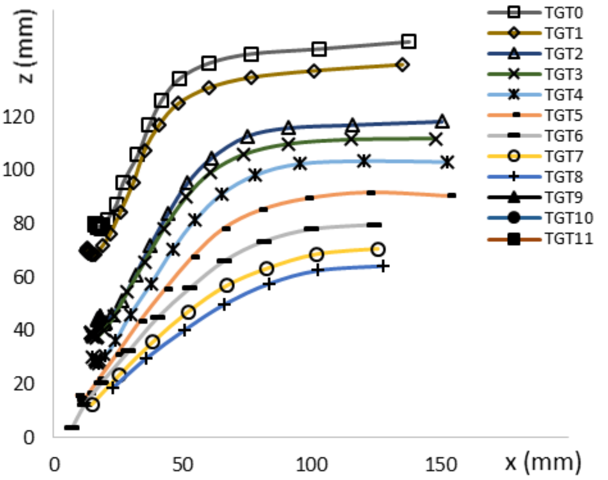

Figure 7. Trajectories of vertebral bodies of PMHS 1 during IIWPG pulse with a head restraint in place

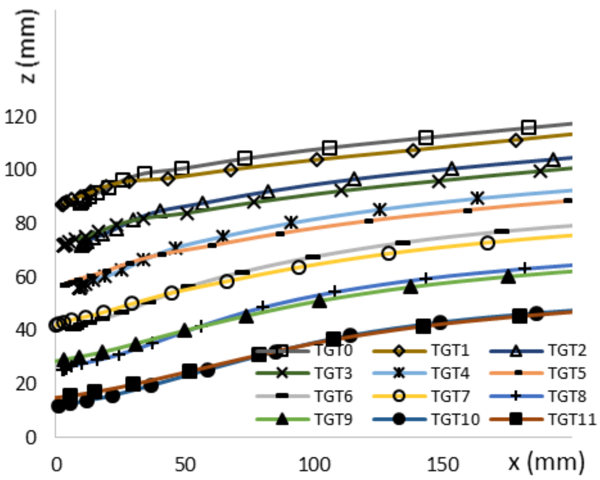

Figure 8. Trajectories of vertebral bodies of FEA simulation representing the test described in Fig.7

The rise of the trajectories of the vertebral bodies of the FEA in Figure 8 is significantly less steep than that of the PMHS in Figure 7. This is explained by an obvious ramping effect of the PMHS during the forward acceleration, which does not occur in the FEA. The vertical motion of the FEA cervical bodies thus is smaller than that of the PMHS. In the graph of the FEA (Figure 8), a point of intersection between two adjacent trajectories can be found (e.g. TGT8 and TGT9). This is explained by the rotation of the vertebral body, where the leading node rises up more than the following node of each vertebral body. In Figure 7 this effect is not visible, since for this specific PMHS only the leading head of the marker could be tracked. Also it can be observed that, for example, the C2 vertebral body in FEA (represented by TGT0 and TGT1 in Figure 8) shows the intersection at an earlier stage than, for example, the C6 (represented by TGT9 and TGT10 in Figure 8). This behaviour can also be found in the graph for the PMHS 4 test configuration 3 where, for example, TGT0 and TGT1 intersect (Appendix 8). In this case TGT0 and TGT1 represent the tip and head of one marker tracked and the rotation of the vertebral body causes the same effect. Trajectories of all tests and relevant simulations can be found in Appendix 2 through Appendix 11. Unfortunately, the radiography of PMHS1 under the IIWPG loading without a head restraint, configuration 2, was not usable. Therefore, no trajectories could be extracted for this test.

For easier comparison, the trajectories were transformed to relative movement graphs. In these graphs, only the relative movement of each tracked vertebral body (or target, where more than one target was tracked for each vertebral body), compared to the corresponding TGT0, is shown. In addition to the subsequent motion graphs, a theoretical circular trajectory with a radius of approximately 85 mm is given as reference.

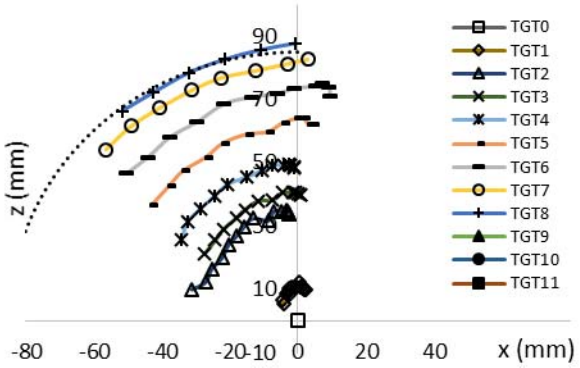

Figure 9. Movement of vertebral bodies of PMHS 1 during SRA 24 km/h pulse without a head restraint

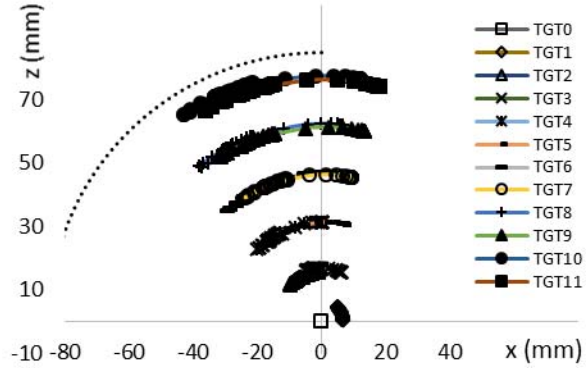

Figure 10. Movement of vertebral bodies of FEA simulation representing the test described in Fig.9

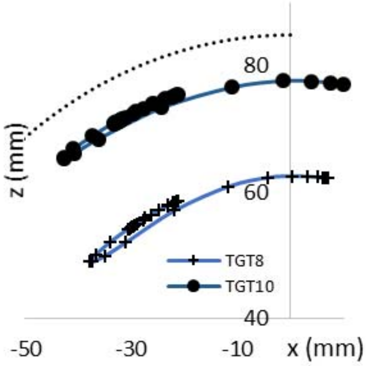

Figure 11. Detail of the "hook-like" rebound motion of the nodes tracked in the FEA analysis.

The movement of the vertebral bodies shows a circular-like motion about the referenced target TGT0 for Figure 9 and Figure 10. In Figure 11 also parts of the rebound movement are displayed which causes a hook-like shape of the single lines on the left-hand side. This motion is not captured in Figure 9 since the PMHS' neck runs out of the picture area of the image intensifier before the rebound motion occurs. In addition, the absence of the head restraint for this test causes a very late rebound. However, the lines in graph Figure 9 and Figure 10 appear to follow a strict circular trajectory about the TGT0 in the C1 vertebral body. All available motion graphs for all PMHS and FEA analysed are found in Appendix 12 through Appendix 21.

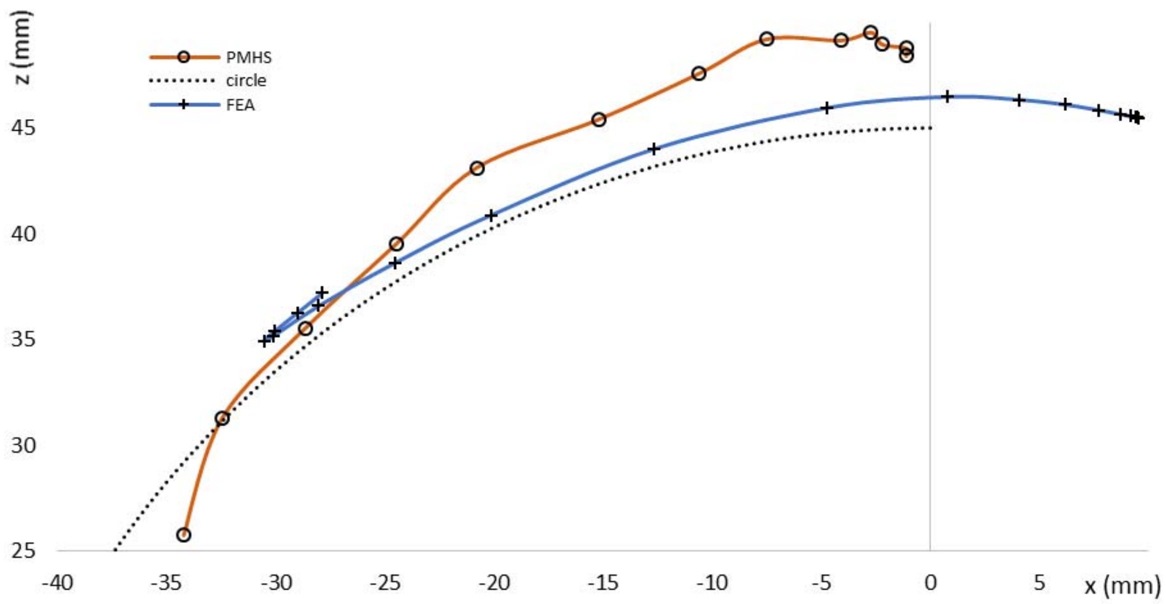

Figure 12. Movement of one target in reference to TGT0 for PMHS1 during SRA 24 km/h pulse without a head restraint compared to the corresponding FEA.

Comparing the trajectory of one vertebral body in detail, e.g. one target at C4 as in Figure 12, little differences in the motion can be found. The trajectory of the FEA follows a motion very similar to the circle indicated as reference (dotted line radius 45 mm). The line of the PMHS on the other hand shows some deviations. Especially on the left end of the line, a variation from a circular trajectory can be found. This compression and elongation behaviour can be observed even more in the following Figure 13 and Figure 14.

For these graphs, the distances between all targets of one PMHS test or FEA, respectively, were computed in reference to the TGT0. The distance of all targets in reference to TGT0 over time was calculated where D02 represents the distance between TGT0 and TGT2, D03 between TGT0 and TGT3 and so on, as illustrated in Figure 6. Furthermore, the initial length at t = 0 ms (e.g. $\underline{D02}_{(t\,=\,0)}$ for TGT2 in Figure 6) of each distance vector was subtracted leading to a graph of relative elongation or compression over time.

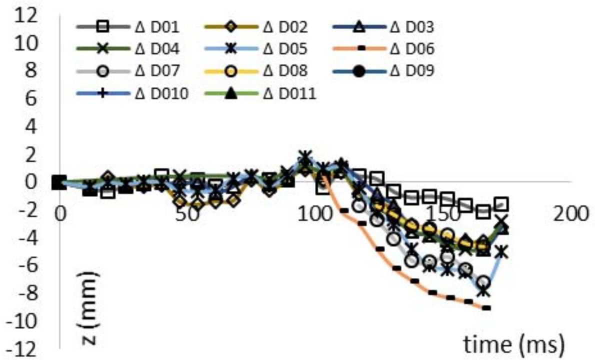

Figure 13. Relative elongation of distance between each target and TGT0 of PMHS1 during IIWPG pulse with a head restraint in place

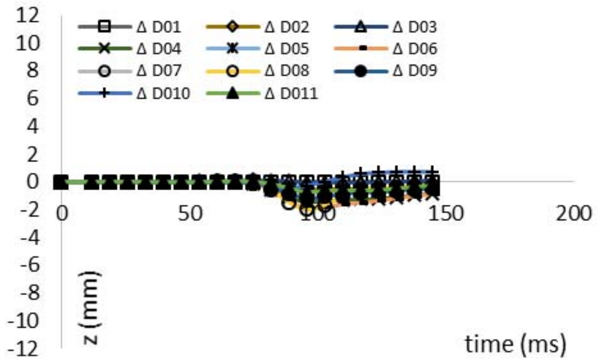

Figure 14. Relative elongation of distance between each target and TGT0 of an FEA during IIWPG pulse with a head restraint

Figure 13 shows some compression around 50 ms and little elongation around 100 ms. Between 120 ms and 150 ms compression of the distances for each target in reference to TGT0 can be found. Figure 14 shows hardly any elongation or compression for the first 80 ms. After that ΔD02 through ΔD07 show compression. However, ΔD010 and ΔD011 after a slight compression between 80 ms and 100 ms show a minor amount of elongation after 100 ms. This behaviour results from the rotational motion of the vertebral bodies of the virtual modelled cervical spine of the EvaRID model.

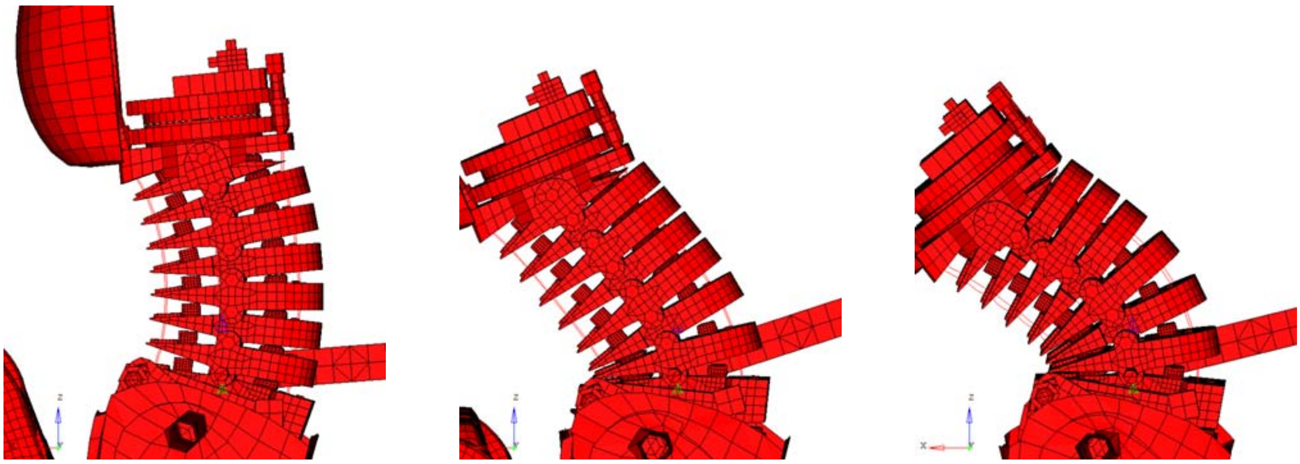

t = 75 ms t = 100 ms t = 125 ms

Figure 15. EvaRID neck model detail under whiplash loading for three different time steps

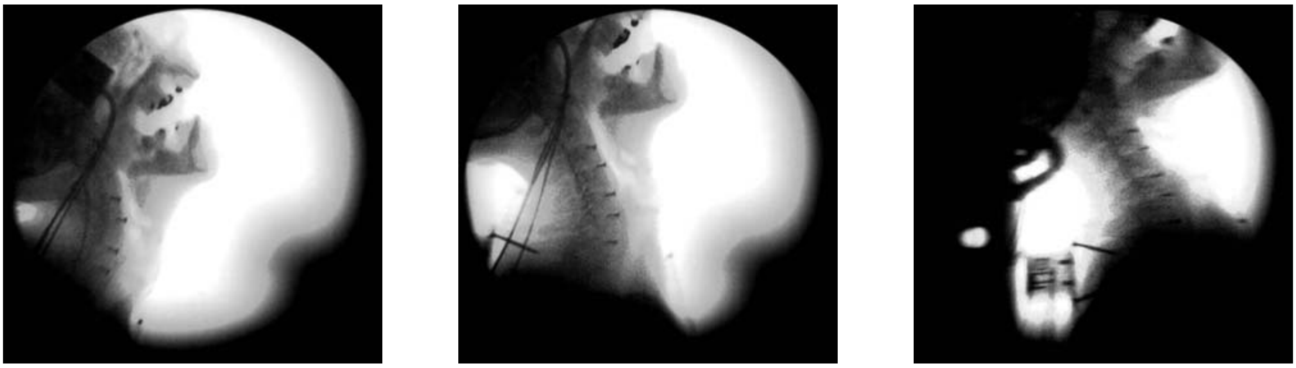

t = 75 ms t = 100 ms t = 125 ms

Figure 16. PMHS neck detail under whiplash loading for three different time steps

Looking at the above Figure 15 for t = 75 ms, the EvaRID neck model appears to be in a shape very much like the initial position with hardly any deformation. The human neck in Figure 16 for t = 75 ms already shows a relatively large amount of extension. Comparing the two pictures for t = 100 ms, a similar overall shape of the neck for the EvaRID and the human neck can be found. For t = 125 ms the shape of the cervical spine of the EvaRID model and human neck differ. Where the neck of the PMHS looks almost straight again, the neck of the EvaRID shows an s-shape. The EvaRID model shows large rotational displacements between C5 to C7. This amount of bending of the neck cannot be found for the PMHS in Figure 16.

In addition, an FEA conducted with the BioRID II (Biofidelic Rear Impact Dummy) model was compared. Interestingly but not unexpected, the virtual BioRID II model, commonly used in vehicle seat development, shows a very similar behaviour in bony kinematics compared to the EvaRID model, as can be found in Figure 17.

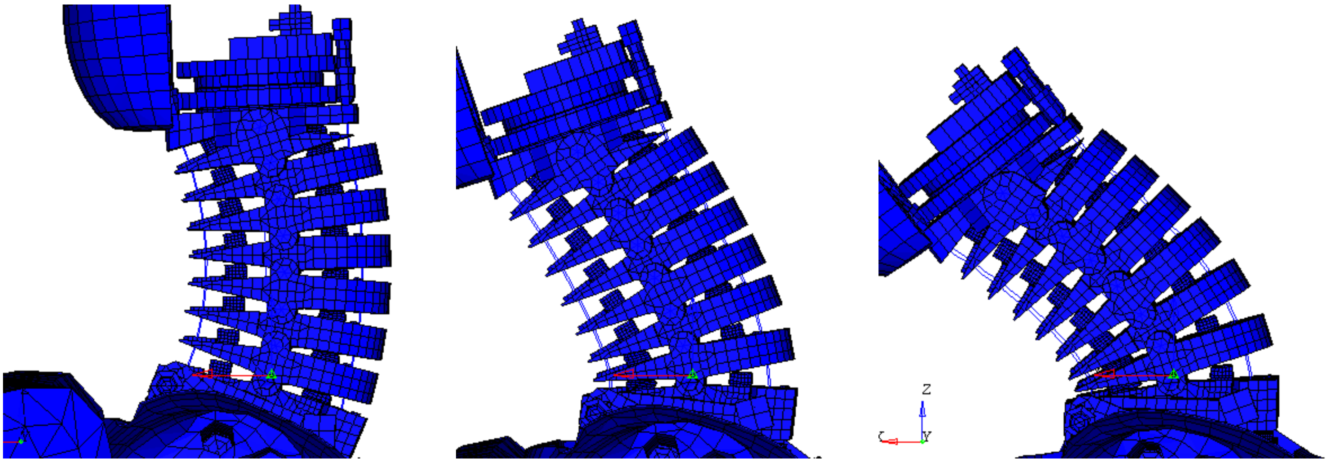

t = 75 ms t = 100 ms t = 125 ms

Figure 17. BioRID neck model detail under whiplash loading for three different time steps

The deformation and shape of the BioRID model's neck looks very much like the behaviour of the EvaRID model. In the following Figure 18 an overlay of the two virtual dummies is displayed. The pictures were scaled to the size of the BioRID to be comparable. Shape and curvature of the cervical spine look similar. The neck of the BioRID seems bent back further, which might be explained by the larger inertia of the head and larger length of the neck. Nevertheless, especially at t =125 ms the rotational motions of the cervical bodies of the BioRID model seems more homogeneous than those of the EvaRID neck.

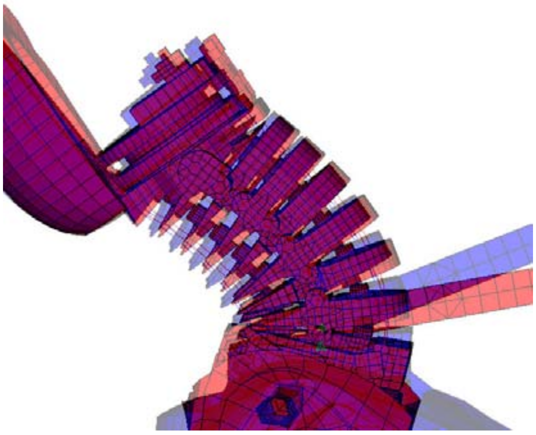

t = 125 ms
Figure 18. Overlay of EvaRID and BioRID cervical spine deformation

T = 125 ms
Figure 19. X-ray picture of male PMHS under the same loading as the FEAs in Figure 18

Looking at Figure 19 the shape of the neck differs for the PMHS tests and FEAs analysed in this study at t = 125 ms. Also differences between the male and female virtual dummy model can be seen in Figure 18.

IV. Discussion

Real world accidents have shown that the risk of sustaining whiplash-associated disorders is higher for females than for males. Within the ADSEAT [15] project, it can be shown that females of average size are associated with the highest whiplash injury frequency [20]. Based on these factors a new virtual rear impact dummy model named EvaRID was developed. The existing BioRID model was scaled to meet anthropometry data of an average female occupant [17, 21]. Two sets of response corridors obtained from female volunteer tests were used for validation [22]. This kind of validation testing is performed at a rather low speed. However, the BioRID and the EvaRID model are used in higher impact speeds, i.e. Euro NCAP whiplash tests with delta-v up to 24 km/h. Within the present study the female model is validated against PMHS tests at Euro NCAP speed levels. Two different female PMHS at four different test set-ups were used. The tests were performed at impact speeds of the IIWPG at 16 km/h and SRA at 24 km/h. Additionally, each test was conducted with and without a head restraint. For comparison, a stiff seat was used to eliminate the influence of seat-bolstering stiffness.

The first results showed a comparable overall kinematic of torso and head. For the kinematics analysis of the cervical spine the motion of markers in the vertebral bodies of the PMHS and corresponding two nodes of the virtual vertebral bodies were compared. A good correlation for a large portion of the whiplash loading for cervical vertebral bodies could be found. However, the bending of the lower neck of the EvaRID model seems excessive. Certainly, the amount of tested female PMHS does not represent a statistically relevant portion of female occupants. Therefore, additional testing is planned. The comparison for male and female PMHSs versus their virtual dummy models indicates that these differences in kinematics occur mainly for the female dummy model.

The comparison with the BioRID virtual model showed a similar behaviour. This was not unexpected because the EvaRID model is a downscaled virtual model of the BioRID. Within the first release of EvaRID only basic scaling adjustments of joint characteristics were made in the EvaRID model. Unfortunately, a comparison of the virtual EvaRID model with a physical EvaRID dummy is currently not feasible.

The amount of testing performed is certainly limiting the extent of validity. For a more general conclusion, additional testing is necessary. In addition, improvements in testing, e.g. increasing the size of the picture intensifier system to gain a larger picture area, would be of great benefit. Furthermore, no general seating procedure for female occupant models, such as the virtual EvaRID dummy model, is currently available.

V. Conclusions

Within the ADSEAT [15] project a virtual female rear-impact dummy model called EvaRID was developed. The model represents a 50th percentile female. EvaRID was already validated against volunteer tests with females. Validation at higher speed levels (i.e. Euro NCAP whiplash testing) was still pending. In this study the EvaRID model was compared with female PMHS rear-impact tests at Euro NCAP medium and high severity loading.

The results show that the virtual rear-impact dummy model EvaRID represents the kinematics of the compared PMHSs well. The indicated deviations could be reduced by further development efforts, e.g. joint stiffness properties and geometry. It would certainly be of value to continue the use of EvaRID for vehicle seat development. Developing a physical dummy, which should be used in rear-impact assessments for female occupants, would be of benefit for the quality of the virtual model as well.

VI. Acknowledgement

Parts of this study were financed by the European Commission as part of the FP7 ADSEAT [15] Project. Additional funding was received from the Styrian federal government.

VII. References

[1] Kihlberg JK. Flexion-torsion neck injury in rear impacts, *Proceedings of 13th AAAM Conference*, 1969, Minneapolis, MN, USA.

[2] O'Neill B, Haddon W, Kelley AB, Sorenson WW. Automobile head restraints—frequency of neck injury claims in relation to the presence of head restraints, *American Journal of Public Health*, 1972, 62(3):399–405.

[3] Thomas C, Faverjon G, Hartemann F, Tarriere C, Patel A, Got C. Protection against rear-end accidents, *Proceedings of IRCOBI Conference*, 1982, Cologne, Germany.

[4] Otremski I, Marsh JL, Wilde BR, McLardy Smith PD, Newman RJ. Soft tissue cervical injuries in motor vehicle accidents, *Injury,* 1989, 20(6):349–351.

[5] Maag U, Desjardins D, Bourbeau R, Laberge-Nadeau C. Seat belts and neck injuries, *Proceedings of IRCOBI Conference*, 1990, Bron, France.

[6] Morris AP, Thomas PD. Neck injuries in the UK Co-operative Crash Injury Study, *Proceedings of 40th Stapp Car Crash Conference*, 1996, Albuquerque, NM, USA, SAE paper no. 962433.

[7] Dolinis J. Risk factors for "Whiplash" in drivers: a cohort study of rear-end traffic crashes, 1997*, Injury,* 1997, 28(3):173–179.

[8] Temming J, Zobel R. Frequency and risk of cervical spine distortion injuries in passenger car accidents: significance of human factors data, *Proceedings of IRCOBI Conference*, 1998, Göteberg, Sweden.

[9] Richter M, Otte D, Pohlemann T, Krettek C, Blauth M. Whiplash-type neck distortion in restrained car drivers: frequency, causes and long-term results, *European Spine Journal*, 2000, 9(2):109–117.

[10] Chapline JF, Ferguson SA, Lillis RP, Lund AK, Williams AF. Neck pain and head restraint position relative to the driver's head in rear-end collisions, *Accident Analysis and Prevention*, 2000, 32(2):287–297.

[11] Krafft M, Kullgren A, Lie A, Tingvall C. The risk of whiplash injury in the rear seat compared to the front seat in rear impacts, *Traffic Injury Prevention*, 2003, 4(2):136–140.

[12] Jakobsson L, Norin H, Svensson MY. Parameters influencing AIS 1 neck injury outcome in frontal impacts, *Traffic Injury Prevention*, 2004, 5(2):156–163.

[13] Storvik SG, Stemper BD, Yoganandan N, Pintar FA. Population-based estimates of whiplash injury using NASS CDS Data, *Biomedical Science Instrumentation*, 2009, 45:244–249.

[14] Kullgren A, Krafft M. Gender analysis on whiplash seat effectiveness: results from real-world crashes, *Proceedings of IRCOBI Conference*, 2010, Hanover, Germany.

[15] Linder A. Adaptive seat to reduce neck injuries for female and male occupants, Internet: http://www.adseat.eu/, April 25th 2013 [March 12th 2014].

[16] Luan F, Yang KH, Deng B, Begeman PC, Tashman S, King AI. Qualitative analysis of neck kinematics during low-speed rear-end impact, *Clinical Biomechanics*, 2000, 15(9):649-657.

[17]Carlsson A, Chang F, et.al. EvaRID - A 50th percentile female rear impact finite element dummy model, *Proceedings of IRCOBI Conference*, 2012, Dublin, Ireland.

[18] Euro NCAP, European New Car Assessment Programme, The Dynamic Assessment of Car Seats for Neck Injury Protection Testing Protocol, Version 3.1, 2011.

[19] United Nations, Regulation No. 16, Agreement Concerning the Adoption of Uniform Technical Prescriptions

for Wheeled Vehicles, Equipment and Parts which can be fitted and/or be used on Wheeled Vehicles and the Conditions for Reciprocal Recognition of Approvals Granted on the Basis of these Prescriptions, Revision 7, 2012.
[20] Linder A, Schick S, et al. ADSEAT – Adaptive Seat to Reduce Neck Injuries for Female and Male Occupants. TRA Conference, April 23-26 2012, Athens, Greece.
[21] Carlsson A. Addressing Female Whiplash Injury Protection - A Step Towards 50th Percentile Female Rear Impact Occupant Models. Chalmers University of Technology, 2012, Göteborg, Sweden, ISBN/ISSN: 978-91-7385-671-3.
[22] Carlsson A, Linder A, Davidsson J, Hell W, Schick S, Svensson M. Dynamic Kinematic Responses of Female Volunteers in Rear Impacts and Comparison to Previous Male Volunteer Tests, *Traffic Injury Prevention*, 2011, 12:347–357.

VIII. APPENDIX

Appendix 1

				Subject ID			
				1	2	3	4
	Gender			Female	Male	Male	Female
	Age		[years]	64	38	57	83
	Body weight		[kg]	54	75	69	70
	Body size		[m]	1.57	1.74	1.71	1.61
1	Hat size		[m]	0.520	0.540	0.555	0.52
2	Chin-occiput circumference		[m]	0.064	0.660	0.69	0.63
2a	Head height		[m]	0.205	0.235	0.215	0.22
2b	Head length		[m]	0.180	0.160	0.18	0.18
2c	Head breadth		[m]	0.153	0.190	0.17	0.16
3	Neck circumference		[m]	0.380	0.325	0.405	0.44
4	Upper arm		[m]	NOVALUE	NOVALUE	0.28	0.31
5	Chest circumference		[m]	0.870	0.860	0.91.5	1.03
6	Chest height		[m]	NOVALUE	NOVALUE	0.22	0.22
7	Chest width		[m]	0.300	0.280	0.29	0.31
8	Abdomen circumference		[m]	0.770	0.780	0.83	1.00
9	Buttocks – Shoulder		[m]	0.580	0.710	0.64	0.58
10	Seat height		[m]	NOVALUE	NOVALUE	0.87	0.84
11a	Pelvis – Knee	Right	[m]	0.450	0.590	0.56	0.53
11b	Pelvis – Knee	Left	[m]	0.450	0.590	0.57	0.53
12a	Sole of foot – Knee	Right	[m]	0.475	0.520	0.52	0.44
12b	Sole of foot – Knee	Left	[m]	0.475	0.520	0.52	0.44
13a	Pelvis – Heel	Right	[m]	0.780	0.930	0.96	0.92
13b	Pelvis – Heel	Left	[m]	0.780	0.930	0.96	0.92
14	Sternum to Chin		[m]	NOVALUE	NOVALUE	0.105	0.08
15a	T1 to Inion (0°)		[m]	NOVALUE	NOVALUE	0.105	0.08
15b	T1 to Inion (flexion)		[m]	NOVALUE	NOVALUE	NOVALUE	NOVALUE
15c	T1 to Inion (extension)		[m]	NOVALUE	NOVALUE	NOVALUE	NOVALUE
16	Hip circumference		[m]	0.870	0.970	NOVALUE	NOVALUE
17	Shoulder width		[m]	NOVALUE	NOVALUE	40	36

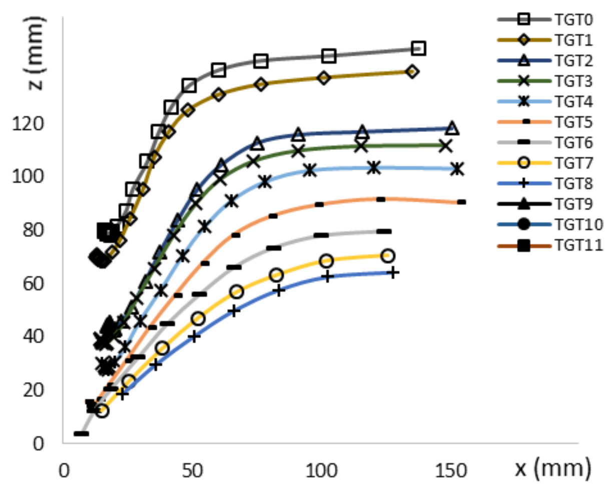

Appendix 2 PMHS1_1 all trajectories tracked

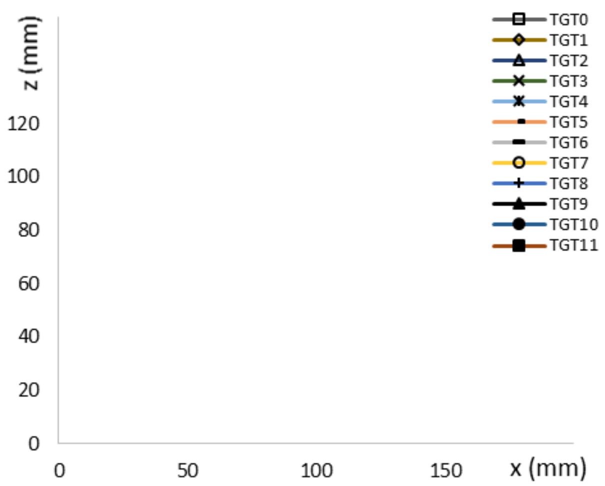

Appendix 3 PMHS1_2 all trajectories tracked

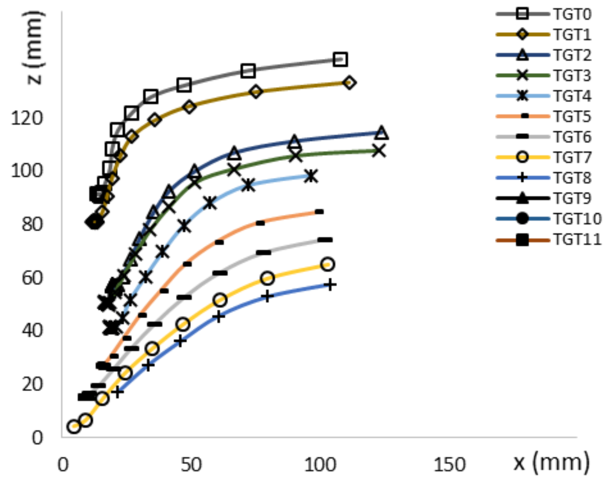

Appendix 4 PMHS1_3 all trajectories tracked

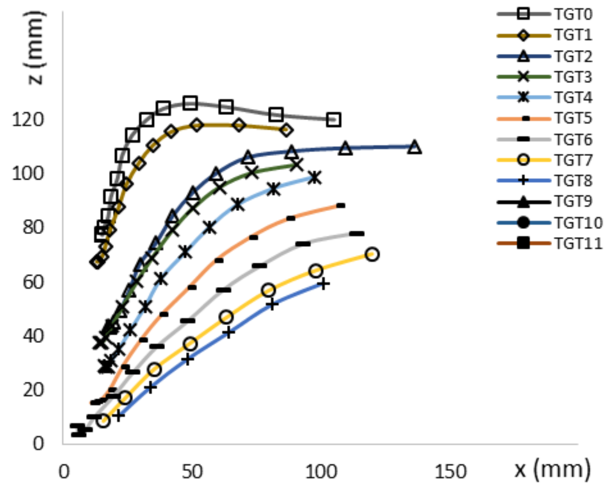

Appendix 5 PMHS1_4 all trajectories tracked

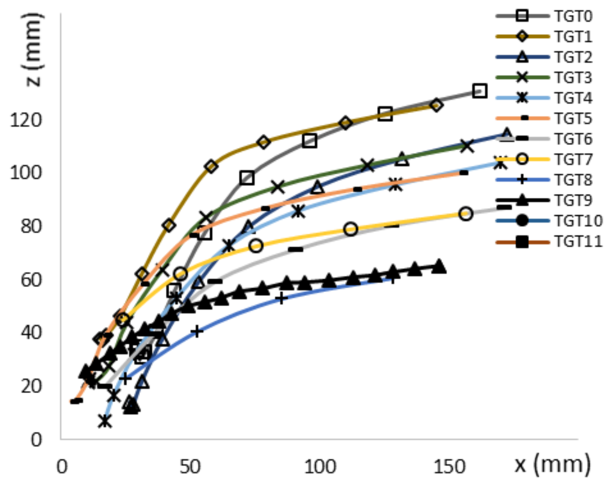

Appendix 6 PMHS4_1 all trajectories tracked

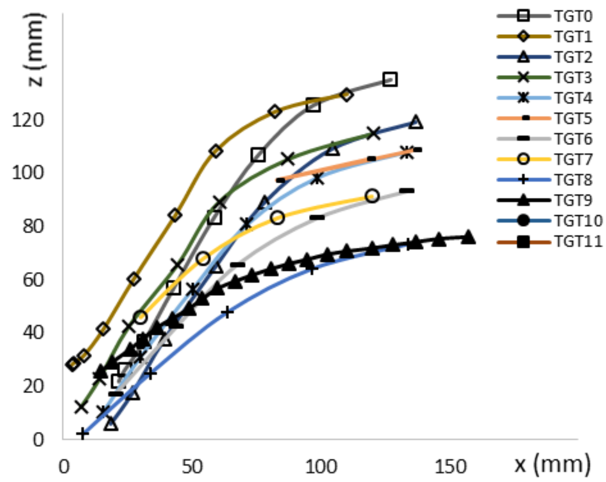

Appendix 7 PMHS4_2 all trajectories tracked

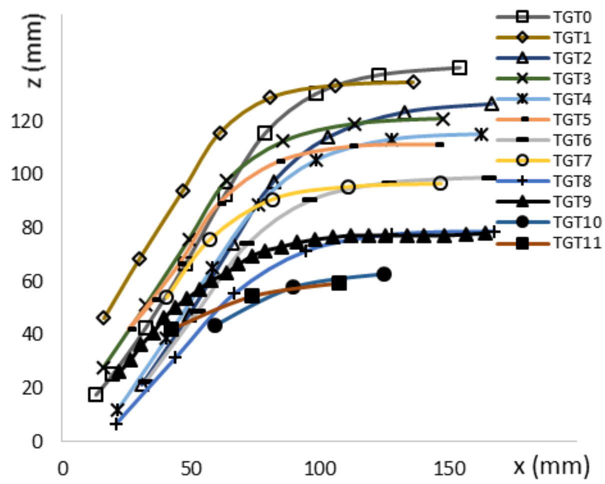

Appendix 8 PMHS4_3 all trajectories tracked

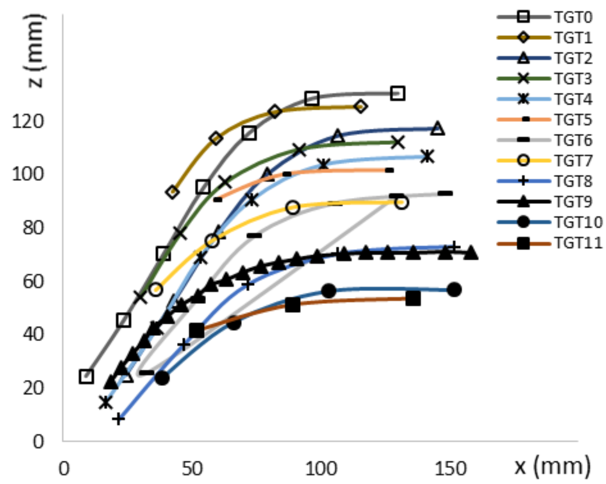

Appendix 9 PMHS4_4 all trajectories tracked

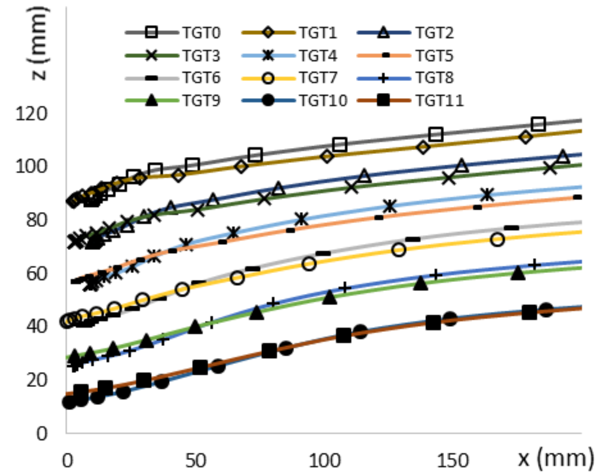

Appendix 10 EvaRID IIWPG all trajectories extracted

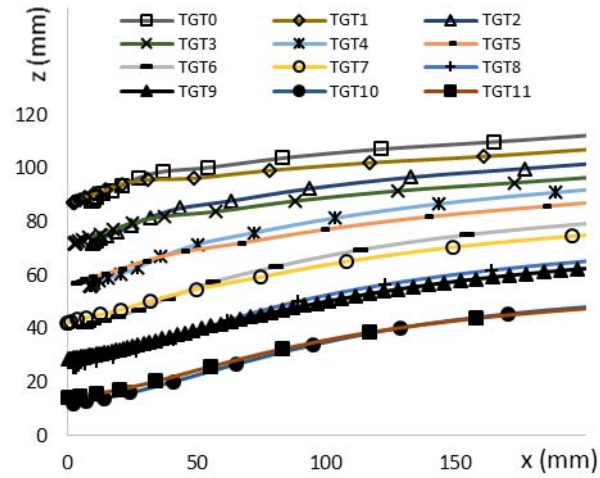

Appendix 11 EvaRID SRA 24 all trajectories extracted

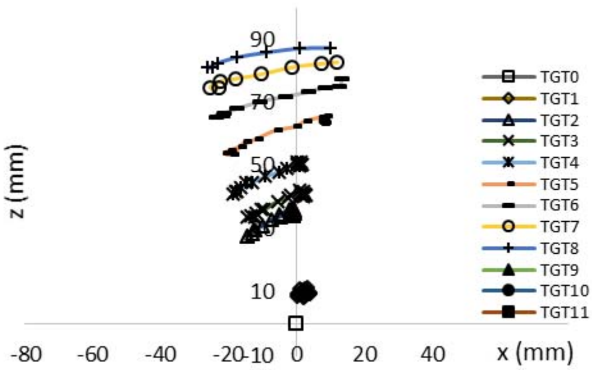

Appendix 12 PMHS1_1 motion of targets about TGT0

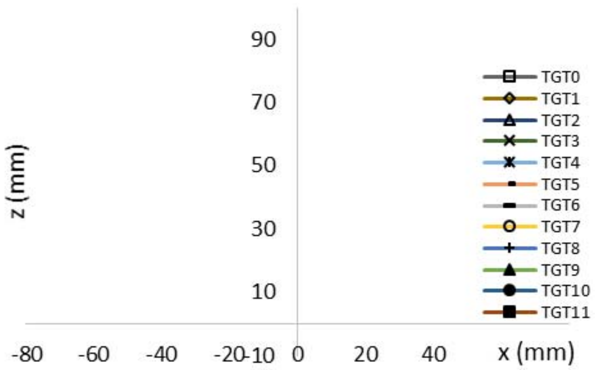

Appendix 13 PMHS1_2 motion of targets about TGT0

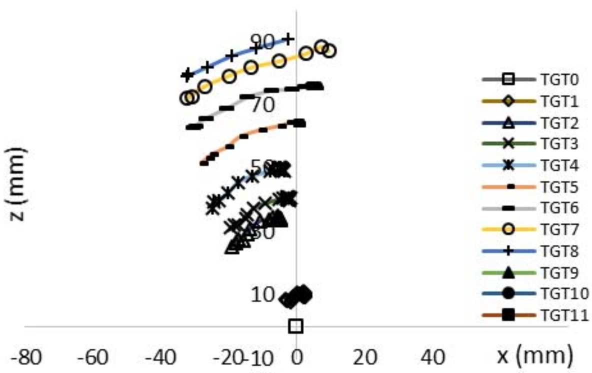

Appendix 14 PMHS1_3 motion of targets about TGT0

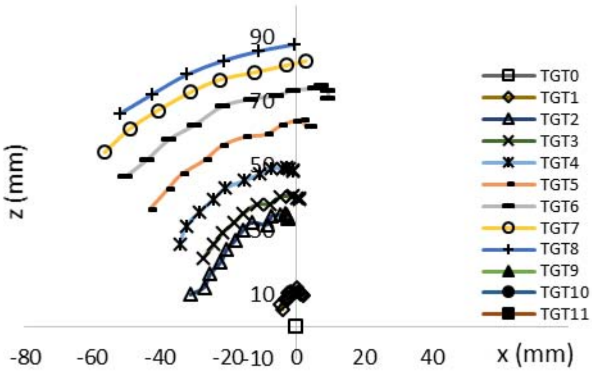

Appendix 15 PMHS1_4 motion of targets about TGT0

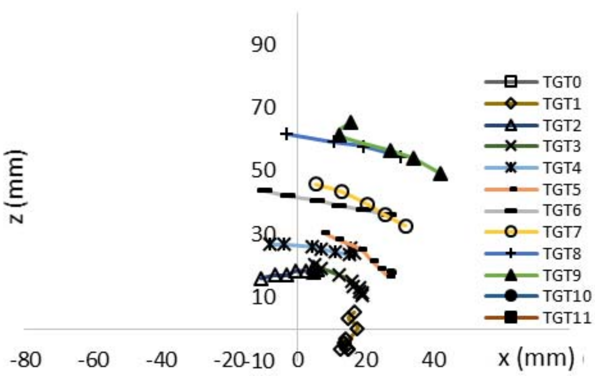

Appendix 16 PMHS4_1 motion of targets about TGT0

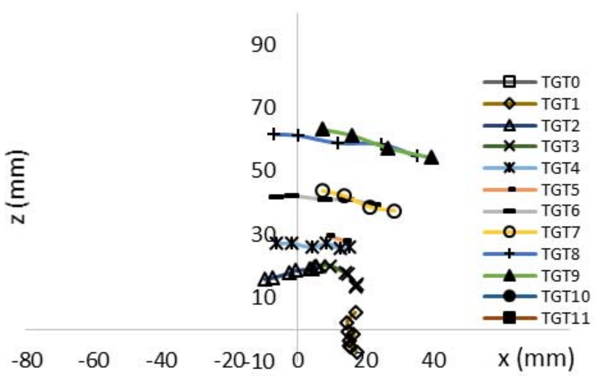

Appendix 17 PMHS4_2 motion of targets about TGT0

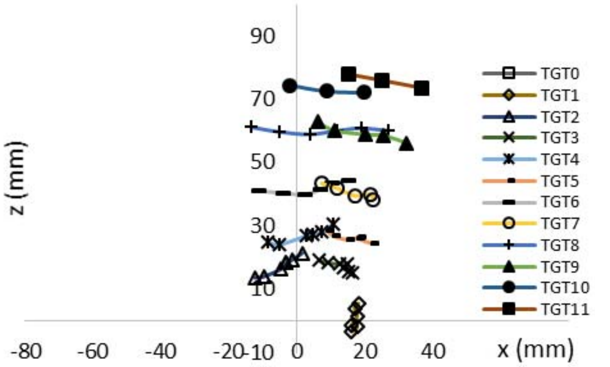

Appendix 18 PMHS4_3 motion of targets about TGT0

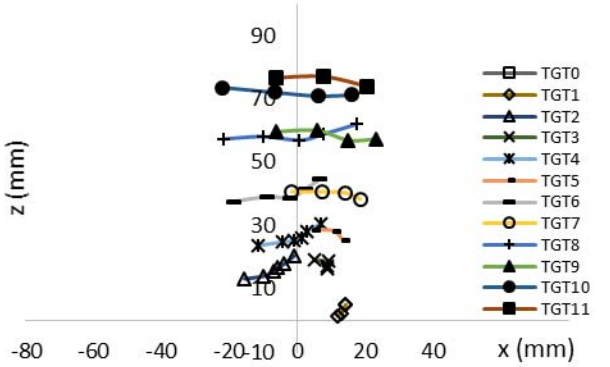

Appendix 19 PMHS4_4 motion of targets about TGT0

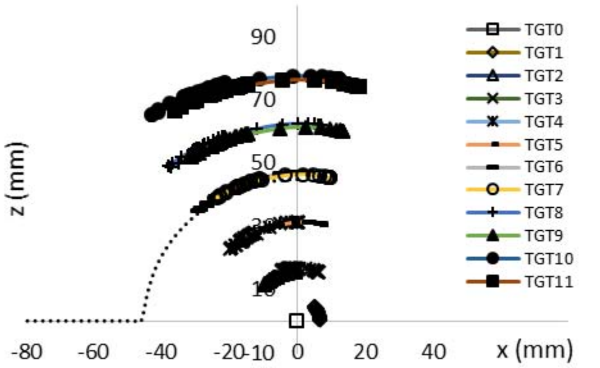

Appendix 20 EvaRID IIWPG motion of targets about TGT0

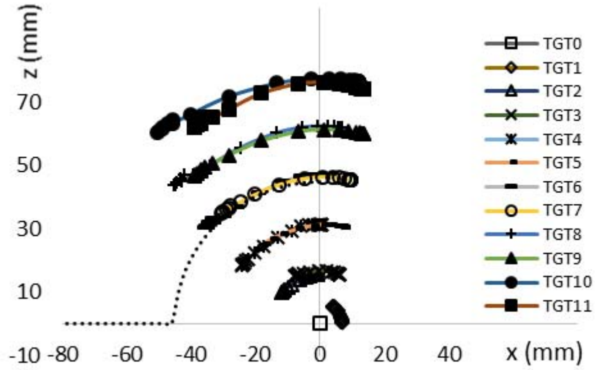

Appendix 21 EvaRID SRA 24 motion of targets about TGT0

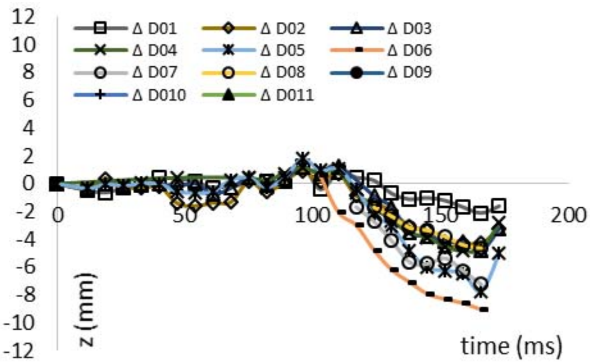

Appendix 22 PMHS1_1 relative elongation in reference to TGT0

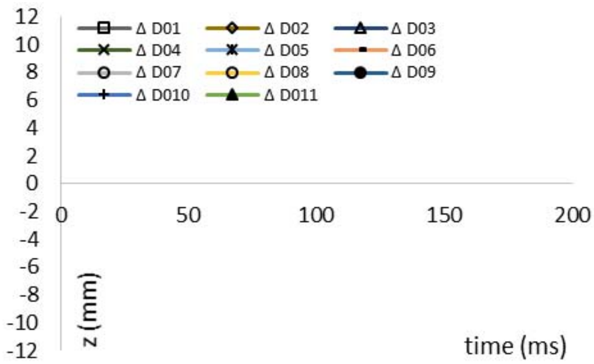

Appendix 23 PMHS1_2 relative elongation in reference to TGT0

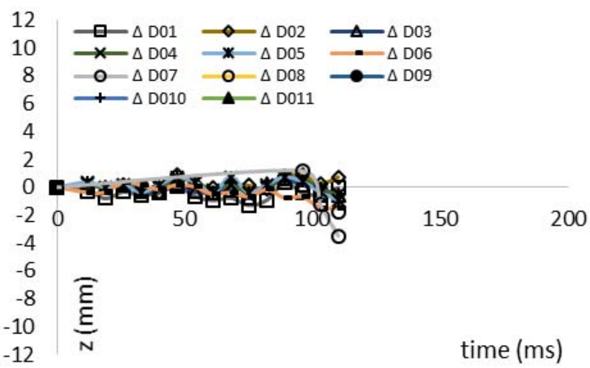

Appendix 24 PMHS1_3 relative elongation in reference to TGT0

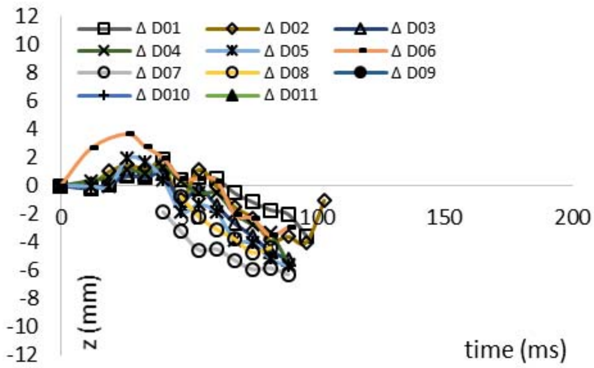

Appendix 25 PMHS1_4 relative elongation in reference to TGT0

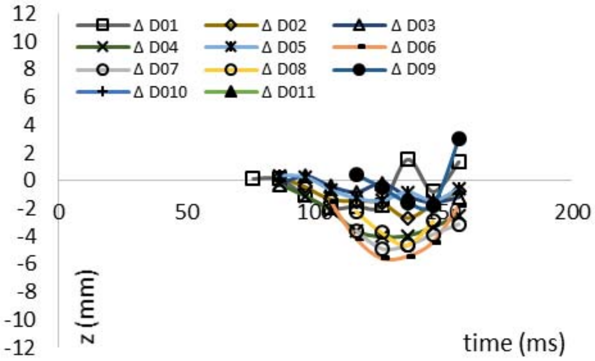

Appendix 26 PMHS4_1 relative elongation in reference to TGT0

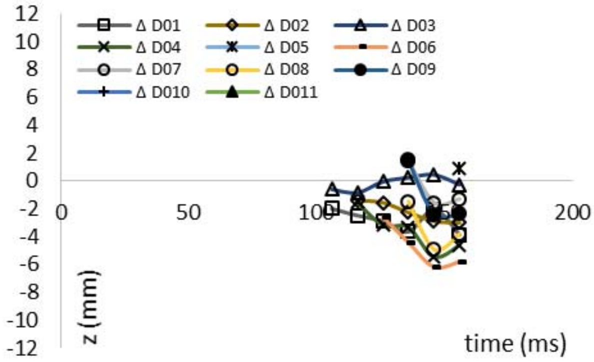

Appendix 27 PMHS4_2 relative elongation in reference to TGT0

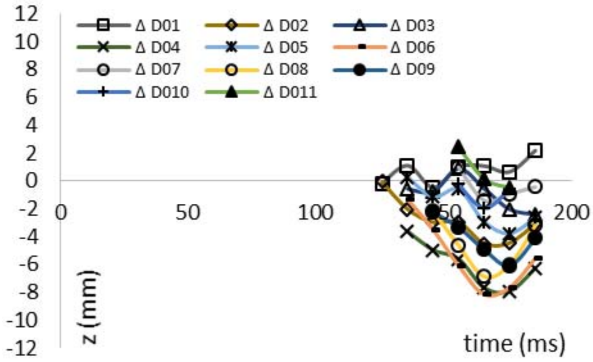

Appendix 28 PMHS4_3 relative elongation in reference to TGT0

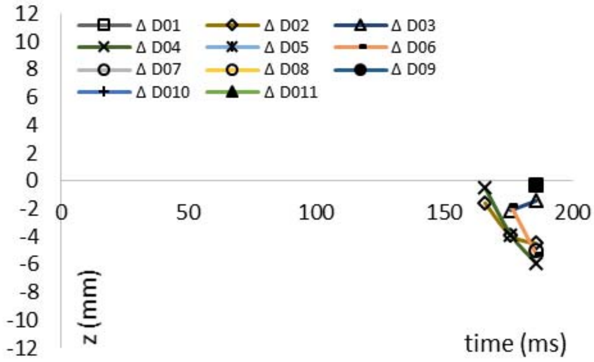

Appendix 29 PMHS4_4 relative elongation in reference to TGT0

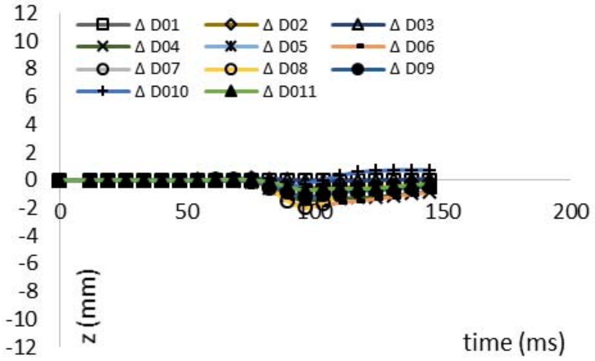

Appendix 30 EvaRID IIWPG relative elongation in reference to TGT0

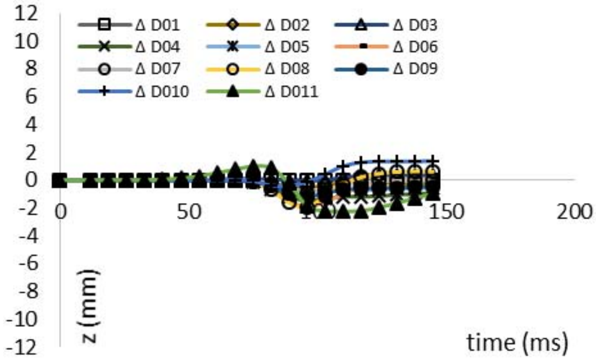

Appendix 31 EvaRID SRA 24 relative elongation in reference to TGT0

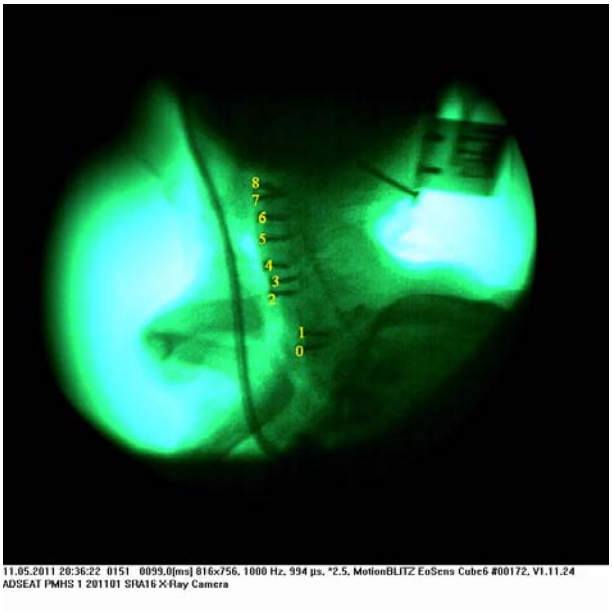

Appendix 32 PMHS1_1 x-ray picture with TGT numbers

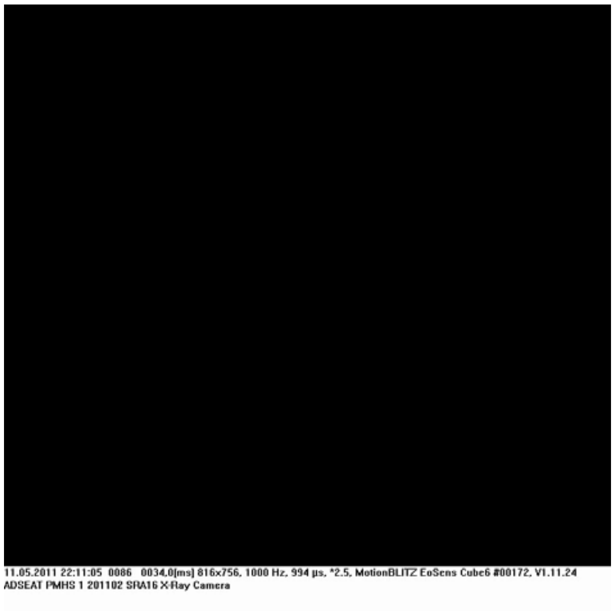

Appendix 33 PMHS1_2 x-ray picture with TGT numbers

Appendix 34 PMHS1_3 x-ray picture with TGT numbers

Appendix 35 PMHS1_4 x-ray picture with TGT numbers

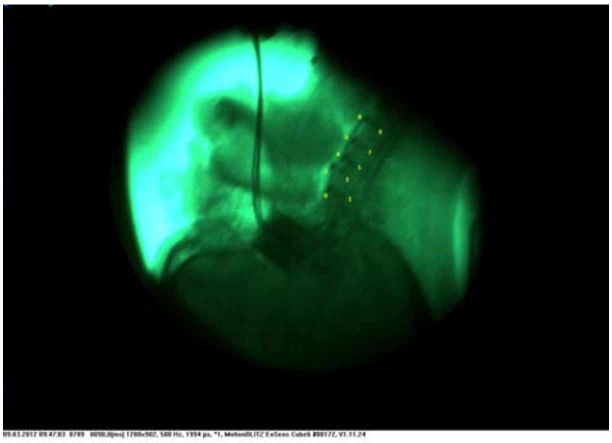

Appendix 36 PMHS4_1 x-ray picture with TGT numbers

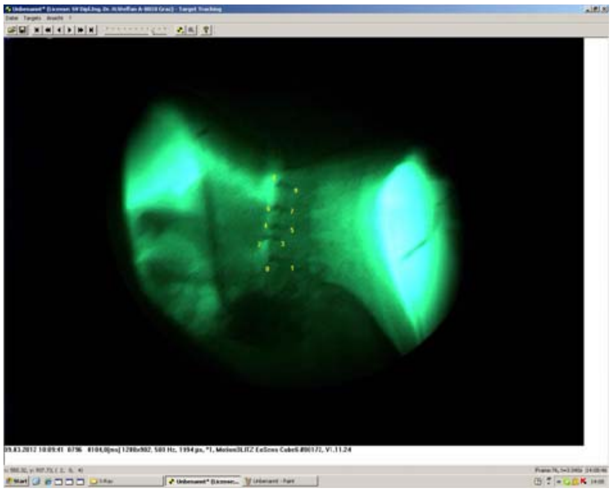

Appendix 37 PMHS4_2 x-ray picture with TGT numbers

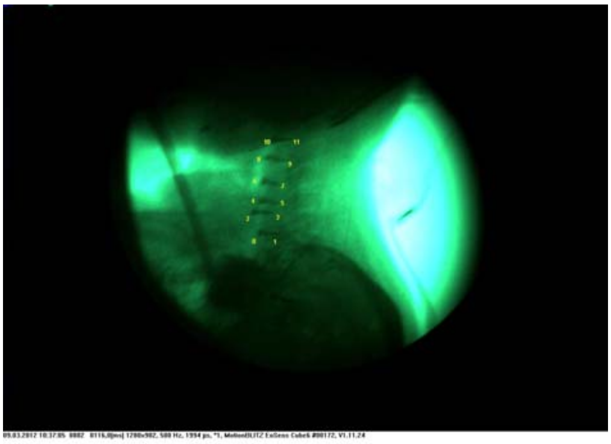

Appendix 38 PMHS4_3 x-ray picture with TGT numbers

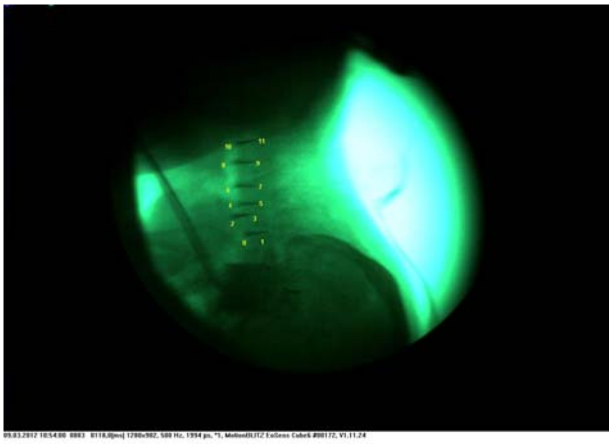

Appendix 39 PMHS4_4 x-ray picture with TGT numbers